Bootstrapping Multi-atlas Hippocampal Segmentation with MAGeT

Pipitone J., Winterburn J., Lerch J., Pruessner J., Lepage M.,
Voineskos A., Chakravarty M.M., and
the Alzheimer's Disease Neuroimaging Initiative

February 15, 2013

Abstract

Neuroimaging research often relies on automated anatomical segmentations of MR images of the brain. Current multi-atlas based approaches provide accurate segmentations of brain images by propagating manually derived segmentations of specific neuroanatomical structures to unlabelled data. These approaches often rely on a large number of such manually segmented atlases that take significant time and expertise to produce. We present an algorithm for the automatic segmentation of the hippocampus that minimizes the number of atlases needed while still achieving similar accuracy to multi-atlas approaches.

finish

1 Introduction

The hippocampus is of particular interest to many researchers because it is implicated in forms of brain dysfunction such as Alzheimer's disease(Sabuncu et al., 2011) and schizophrenia(Narr et al., 2004; Karnik-Henry et al., 2012), and has functional significance in cognitive processes such as learning and memory(den Heijer et al., 2012; Scoville and Milner, 2000). For many research questions involving magnetic resonance imaging (MRI) data accurate identification of the hippocampus and its subregions is a necessary first step to better understand the individual neuroanatomy of subjects.

Currently, the gold standard for neuroanatomical segmentation is manual delineation by an expert human rater. This is problematic for hippocampal segmentation for several reasons. First, manual segmentation takes a significant investment of time and expertise (Hammers et al., 2003) which may not be readily available to researchers or clinicians. Second, the amount of data produced in neuroimaging experiments increasingly exceeds the capacity for identification of specific neuroanatomical structures by an expert manual rater. Third, the true definition of hippocampal anatomy in MR images is disputed (Geuze et al., 2004), as evidenced by efforts to create an unified segmentation protocol (Jack et al., 2011).

Compounding each of these problems is the significant neuroanatomical variability in the hippocampus throughout the course of aging, maturation, and neuropsychiatric disorders (?Sabuncu et al., 2011; ?; Gogtay et al., 2006; Narr et al., 2002). The result is that existing hippocampal atlases available to a researcher may not accurately represent neuroanatomy of a specific population under study. Additionally, in the course of a research or clinical study, it may be necessary to make adjustments to hippocampal definition as a means of hypothesis testing. For example, Poppenk (Poppenk and Moscovitch, 2011) found that subdividing the hippocampus into anterior and posterior regions resulted in a predictive relationship between volume difference of those regions and recollection memory performance. Making such modifications to a set of MRI data segmentations requires additional manual effort.

Automated segmentation techniques do not require human intervention but do require *a priori* anatomical information to guide segmentations. In this paper we focus on methods that use manually segmented MRI atlases as anatomical priors, as these methods achieve some of the best automated hippocampal segmentation accuracies to-date. This technique was first developed using a single atlas prior (known as single-atlas, or model-based, segmentation). Volumetric image registration is used to estimate between the

1

neuroanatomy of an atlas and target images. Labelling of the target image is achieved by applying the resulting transformation to the atlas labels to bring them into the target image space (*label propagation*). This method is limited in accuracy by the introduction of estimation errors in registration and partial volume effects in label resampling, and errors introduced when the anatomy of the atlas is unrepresentative of the target anatomy.

Multi-atlas segmentation techniques address these limitations by combining segmentation information from a series of expertly segmented atlases (Heckemann et al., 2006, 2011; Collins and Pruessner, 2010; **?**; Aljabar et al., 2009; Leung et al., 2010; Wolz et al., 2010). Each atlas image is registered to a target image, and label propagation is performed to produce several labellings of the target image (one from each atlas). A *label fusion* technique, such as voxel-wise voting, is used merge these labels into a definitive segmentation for the target. In addition, *atlas selection* techniques are often used to exclude atlases from label fusion that are dissimilar to a target image in order to reduce error from unrepresentative anatomy (Aljabar et al., 2009). Cross-correlation or normalised mutual information of image intensities are common measures of image similarity used in atlas selection.

Multi-atlas methods have been very successfully applied to hippocampal segmentation. Collins et al. found near-manual segmentation performance using an atlas library of 80 T1-weighted atlas images from the ICBM152 dataset, the ANIMAL nonlinear registration algorithm, normalised mutual information as an atlas selection similarity metric, and majority vote for label fusion (Collins and Pruessner, 2010). The Alzheimer's Disease Neuroimaging Initiative (ADNI) is a commonly used benchmarking dataset of MR images of controls and patients with MCI or Alzheimer's (see Methods for more information on the ADNI dataset. Leung et al. tuned parameters for registration and label fusion to the segmentation of ADNI1 1 year dataset of images with an atlas library of 55 images (Leung et al., 2010). The MAPER whole brain segmentation algorithm (Heckemann et al., 2006, 2011), using 30 atlases, on all ADNI1 baseline images (Heckemann et al., 2011). Lotjonen et al. use images from the ADNI1 baseline dataset and 30 atlases with a proprietary non-linear registration method based on intensity differences, a post-processing step using a graph cuts algorithm to optimise fused segmentations against a spatial intensity prior (**?**). No story here

The LEAP algorithm is an elegant modification to the basic multi-atlas strategy (Wolz et al., 2010). The atlas library is grown, beginning with a set of manually labelled atlases, and successively incorporats unlabelled target images after being labelling using multi-atlas techniques. The sequence in which target images are labelled is chosen so that the similarity between the atlas images and the target images is minimised at each step, effectively allowing for deformations between very dissimilar images to be broken up into sequences of smaller deformations. With an atlas library of 30 MR images, LEAP was used to segment the ADNI1 baseline dataset, achieving a mean Dice score of 0.85 with manual segmentations.

While not purely multi-atlas techniques, there are several important algorithms for hippocampal segmentation that inform our approach. The popular FreeSurfer application's whole brain segmentation algoritm uses a probabilistic atlas of anatomical and tissue classes along with spatial constraints for class labels encoded using a Markov random field model (Fischl et al., 2002). When segmenting hippocampal subfields, FreeSurfer employs a Bayesian inference algorithm using a probabilistic atlas of anatomical classes as a prior, and a likelihood model of how those classes translate into MR image intensities, both trained on manual segmentations of high resolution MR images (**?**). Yushkevitch et al. describe a semi-automated method for hippocampal subfield segmentation of focal T2 images(**?**). The unlabelled MR image must be manually partitioned into 'head', 'body' and 'tail', and then multi-atlas methods are used to segment the image. Finally, an AdaBoost-based bias correction classifier is trained on texture, spatial location, and intensities of manual segmentations and is applied to fix mislabelled voxels.

Aside from the algorithmic choices used in multi-atlas segmentation, it is natural to ask about how the features of the atlases themselves impact the resulting segmentations. As noted, by choosing atlases ranked most similar to a target image by voxel intensity profile, segmentation accuracy is improved, suggesting that neuroanatomical similarity plays a strong role (Aljabar et al., 2009). Carmichael et al. explored this directly and found that when using only one atlas the important factors leading to improved accuracy are that the atlas have neuroanatomical features that match the target, and that the atlas segmentation use the same protocol as the gold-standard (Carmichael et al., 2005). Nestor et al. found that hippocampal segmentation protocols that include more dorsal white-matter and posterior anatomy tended to produce higher overlap and better accuracy at distinguishing disease classes in the ADNI1 1 year dataset (Nestor et al., 2012). These results suggest both atlas library neuroanatomy and delineation protocol play a significant role in the

resulting segmentation.

Considered along with our earlier discussion on the difficulty of producing manual segmentations of MR images and the need for adaptable segmentation definitions in order to conduct research, this presents a real problem of labour and expertise when using existing multi-atlas segmentation methods which rely on relatively large atlas libraries (typically between 30 and 80 atlases). Indeed, it may be especially prohibitive to use these methods in situations where producing a single atlas is challenging (e.g. histology-based atlases, or atlases from very high resolution images). In this paper we address the problem of producing accurate segmentations using small numbers of manually segmented atlases.

Our algorith, called MAGeT brain (*M*ultiple *A*utomatically *G*enerated *T*emplates), is an extension to the basic multi-atlas-based segmentation schema(**?**). Principally, we explore the possibility of using a small atlas library to bootstrap a much larger *template library* composed of images taken from the target population. The template library is then used to segment the targets in a similar fashion to basic multi-atlas segmentation: by label propagation and label fusion. The intuition driving this approach is that by generating a template library we leverage the unique neuroanatomy target population on hand to initialize the segmentation process and improve accuracy over direct propagation from the atlas library to unlabelled targets while also using fewer manually segmented atlases.

The insight of generating a template library is not new. Heckemann et al. compared "indirect" segmentation – taking a single atlas and propagating the labels to intermediate targets before fusing them in a target image space – to multi-atlas segmentation and found that the indirect approach performed worse (Heckemann et al., 2006). In this paper we continue the same line of investigation but explore the performance when using multiple atlases as well as the effect of different registration and fusion methods.

The LEAP algorithm (Wolz et al., 2010), described above, is another example of indirect segmentation previously explored. LEAP proceeds by iteratively segmenting unlabelled images most similar to the atlas library images and then incorporating the labelled images into the atlas library for future iterations. The novelty explored in current work is to demonstrate the viability of achieving comparable segmentation accuracy using the basic multi-atlas schema and using significantly fewer manually created atlases.

In previous work (**?**), we applied MAGeT brain to segmentation of the human striatum, globus pallidus, and thalamus using a single histologically-derived atlas. The contribution of the present work is to extend our approach to the human hippocampus and perform a series of experiments to rigorous validate the method. First, we conduct an extensive cross-validation of MAGeT and basic multi-atlas segmentation on a subset of the ADNI1 dataset to assess the accuracy of MAGeT brain under various parameter settings (number of atlases and templates, registration and fusion methods). With the best performing parameter configuration discovered above, we estimate MAGeT intra-rater reliability by segmenting separately acquired T1 images of the atlas subjects. For this experiment, we use the Winterburn atlases: digital hippocampal subfield segmentations of five in-vivo high-resolution (300u isotropic) T1-weighted MR scans. To validate MAGeT in a real world situation, we segment the entire ADNI1 screening dataset and compare our segmentations to established automated and manual segmentations. Additionally, to ensure MAGeT brain accuracy across disease categories, we also compare MAGeT segmentations to manual segmentations of 139 first episode schizophrenic patients.

2 Methods

2.1 MAGeT Brain Algorithm

In this paper we will be making a distinction between an atlas and a template – typically these terms are used roughly interchangeably. The term *atlas* is taken to refer to two image volumes: an intensity image (*atlas image*) and a corresponding manual segmentation image (*atlas labels*). *Template* refers more generically to any image and corresponding labelling, manual or computed, when it is *used as* as a model in the segmentation of another image. The terms *atlas library* and *template library* mean a set of such images. Additionally, we will use the terms *target* to refer to an intensity image for which we would like an segmentation.

The simplest form of multi-atlas segmentation combines labellings derived from several atlases by way of label fusion (Heckemann et al., 2006, 2011). We will refer to this as *basic multi-atlas segmentation*. The schema as for this method is as follows:

1. An atlas library and set of target images are given as input. The atlas library is used as a template library in the following steps;

2. Each atlas intensity image is nonlinearly registered to each target intensity image;

3. Label images from each atlas are propagated via the resulting transformations to the target image space; and

4. the resulting labels are fused to produce a single, definitive segmentation.

The particular registration and voting method used are left unspecified.

MAGeT brain is best understood as an extension of the basic multi-atlas segmentation schema. Instead of using the atlas library to directly label the target images, a subset of the input images are selected as template images and then labelled. The choice of targets used in the template library can be made to reflect the neuroanatomy or demographics of the target set as a whole (for instance, by sampling equally from cases and controls). Once the template library images have been chosen, a truncated version of basic multi-atlas segmentation is used to label the template library images without performing label fusion. Instead, each template image receives multiple labellings: one from each atlas image. A second round of basic multi-atlas segmentation uses the template library to segment the entire set of target images (including those images used in the template library). Label fusion in this final step fuses all labels from all templates. To summarize, figure 1 describes the MAGeT brain algorithm in pseudocode.

Source code for MAGeT brain can be found at http://github.com/pipitone/MAGeTbrain

---

Algorithm 1 Pseudocode for the MAGeT Brain algorithm

```
function BasicMultiAtlasSegmentation(Templates, Subjects)
    for all target do
        for all template do
            propagate all labels for template to target space
            store target labels
        end for
        fuse target labels
    end for
end function

function MAGeTBrain(Subjects, Atlases, n)
    for i = 1 → n do
        choose a target to be used as a template
        propagate labels from each atlas to template space
        store the template with all of its labels
    end for
    MultiAtlas(Templates, Subjects)
end function
```

2.2 Subjects

Our experiments use three distinct subject datasets.

2.2.1 ADNI1 1.5T Screening Dataset

Clinical, demographic and pre-processed T1-weighted MRI were downloaded by the authors from the ADNI1 database (adni.loni.ucla.edu) between March 2012 and August 2012. The image dataset download was the "ADNI1:Screening 1.5T" standardized dataset available from ADNI [1] (Wyman et al., 2012). This image collection contains uniformly preprocessed images which have been designated to be the "best" after quality control. All images were acquired using 1.5T scanners (General Electric Healthcare, Philips Medical Systems or Siemens Medical Solutions) at multiple sites using the protocol described in (**?**). Representative 1.5T imaging parameters were TR = 2400ms, TI = 1000ms, TE = 3.5ms, flip angle = 8∘, field of view = 240 x 240mm, a 192 x 192 x 166 matrix (x, y, and z directions) yielding a voxel resolution of 1.25 x 1.25 x 1.2 mm^3. Clinical and demographic data are shown in table **??**.

---

[1] http://adni.loni.ucla.edu/methods/mri-analysis/adni-standardized-data/

Table 1: ADNI1 1.5T Screening dataset demographics

	N	CN $N = 229$	LMCI $N = 404$	AD $N = 192$	Combined $N = 825$
Age at baseline Years	825	72.3 75.5 78.5	69.9 74.9 80.4	70.8 75.8 81.0	71.1 75.3 80.0
Sex : Female	825	48% (110)	36% (144)	47% (91)	42% (345)
Education	825	14.0 16.0 18.0	14.0 16.0 18.0	12.0 15.5 16.0	13.0 16.0 18.0
Ethnicity : Unknown	825	1% (3)	1% (4)	1% (2)	1% (9)
Not Hisp/Latino		98% (224)	96% (386)	97% (186)	96% (796)
Hisp/Latino		1% (2)	3% (14)	2% (4)	2% (20)
CDR-SB	825	0.0 0.0 0.0	1.0 1.5 2.0	3.0 4.0 5.0	0.0 1.5 3.0
ADAS 13	816	6.00 9.33 12.33	14.33 18.33 23.00	23.41 28.50 34.00	11.00 17.67 24.00
MMSE	825	29.0 29.0 30.0	26.0 27.0 28.2	22.0 23.0 25.0	25.0 27.0 29.0

$a \ b \ c$ represent the lower quartile a, the median b, and the upper quartile c for continuous variables.
N is the number of non–missing values.
Numbers after percents are frequencies.

Table 2: Schizophrenia First Episode Patient Demographics

	N	FEP $N = 81$
Age	80	21 23 26
Gender : M	81	63% (51)
Handedness : ambi	81	6% (5)
left		5% (4)
right		89% (72)
Education	81	11 13 15
SES : lower	81	31% (25)
middle		54% (44)
upper		15% (12)
FSIQ	79	88 102 109

$a \ b \ c$ represent the lower quartile a, the median b, and the upper quartile c for continuous variables.
N is the number of non–missing values.
Numbers after percents are frequencies.

For a subset of ADNI1 images, labels of the left and right hippocampi are available (herein refered to as labels). Semi-automated hippocampal volumetry was carried out using a commercially available high dimensional brain mapping tool (Medtronic Surgical Navigation Technologies, Louisville, CO), that has previously been validated and compared to manual tracing of the hippocampus (Hsu et al., 2002). Measurement of hippocampal volume is achieved first by placing manually 22 control points as local landmarks for the hippocampus on the individual brain MRI data: one landmark at the hippocampal head, one at the tail, and four per image (i.e., at the superior, inferior, medial and lateral boundaries) on five equally spaced images perpendicular to the long axis of the hippocampus. Second, fluid image transformation is used to match the individual brains to a template brain (Christensen et al., 1997). The pixels corresponding to the hippocampus are then labeled and counted to obtain volumes. This method of hippocampal voluming has a documented reliability of an intraclass coefficient better than .94 (Hsu et al., 2002).

2.2.2 Schizophrenic First Episode Patients

SFEP dataset demographics are shown in table 2.

2.2.3 Winterburn Atlases

The Winterburn atlases (**?**) are digital hippocampal segmentations of of five in-vivo 300u isotropic T1-weighted MR images. The segmentations include subfield segmentations for the cornus ammonis (CA) 1, CA4, dentate gyrus, subiculum, and CA 2 and 3 combined. Subjects in the Winterburn atlases range in age from 29-57 years (mean age of 37), and include two males and three females.

In addition to the high-resolution scans distributed as part of the Winterburn atlases, we also obtained additional T1 BRAVO scans of four of the five subj

Table 3: ANIMAL Registration Parameters

Parameters	Stage 1	Stage 2	Stage 3
Model Blur (FWHM)	8	8	4
Input Blur (FWHM)	8	8	4
Iterations	30	30	10
Step	8x8x8	4x4x4	2x2x2
Sub-Lattice	6	6	6
Lattice Diameter	24x24x24	12x12x12	6x6x6

2.3 Registration Methods

Before registration, all images underwent preprocessing with the N3 algorithm (Sled et al., 1998) to minimize intensity nonuniformity. In our experiments we use one of two non-linear image registration methods.

2.3.1 Automatic Normalization and Image Matching and Anatomical Labeling (ANIMAL)

The ANIMAL algorithm carries out image registration is in two phases. In the first, a 12-parameter linear transformation (3 translations, rotations, scales, shears) is estimated between images using an algorithm that maximizes the correlation between blurred MR intensities and gradient magnitude over the whole brain (Collins et al.). In the second phase, nonlinear registration is completed using the ANIMAL algorithm (Collins et al., 1995): an iterative procedure that estimates a 3D deformation field between two MR images. At first, large deformations are estimated using blurred version of the input data. These larger deformations are then input to subsequent steps where the fit is refined by estimating smaller deformations on data blurred with a Gaussian kernel with a smaller FWHM. The final transformation is a set of local translations defined on a bed of equally spaced nodes that were estimated through the optimization of the correlation coefficient. For the purposes of this work we used the regularization parameters optimized in Robbins et al. (Robbins et al., 2004), displayed in table 3.

2.3.2 Automatic Normalization Tools (ANTS)

ANTs is a diffeomorphic registration algorithm which provides great flexibility over the choice of transformation model, objective function, and the consistency of the final transformation. The transformation is estimated in a hierarchical fashion where the MRI data is subsampled, allowing large deformations to be estimated and successively refined at later hierarchical stages (where the data is subsampled to a finer grid). The deformation field and the objective function are regularized with a Gaussian kernel at each level of the hierarchy. The ANTs algorithm is freely available http://www.picsl.upenn.edu/ANTS/. We used an implementation of the ANTS algorithm compatible with the MINC data format, mincANTS https://github.com/vfonov/mincANTS.

We used the following command line when running ANTS:

```
mincANTS 3 -m PR[target_file.mnc,source_file.mnc,1,4]
  --number-of-affine-iterations 10000x10000x10000x10000x10000
  --affine-gradient-descent-option 0.5x0.95x1.e-4x1.e-4
  --use-Histogram-Matching --MI-option 32x16000
  -r Gauss[3,0] -t SyN[0.5] -i 100x100x100x20
  -o transformation.xfm
```

se settings were adapted from the "reasonable starting point" given in the ANTS manual [2].

2.4 Label Fusion

Label fusion is a term given to the process of combining the information from several candidate labellings for an intensity image into a single labelling. In this paper we explore three fusion methods.

---

[2]https://sourceforge.net/projects/advants/files/Documentation/

2.4.1 Voxel-wise Majority Vote

Labels are propagated from all template library images to a target. Each output voxel is given the most frequent label at that voxel location amongst all candidate labellings. Ties are broken arbitrarily.

2.4.2 Cross-correlation Weighted Majority Vote

An optimal combination of targets from the template library has previously been shown to improve segmentation accuracy (Aljabar et al., 2009; Collins and Pruessner, 2010). In this method, each template library image is ranked in similarity to each unlabelled image by the normalized cross-correlation (CC) of image intensities after linear registration, over a region of interest (ROI) generously encompassing the hippocampus. Only the top ranked template library image labels are used in a voxel-wise majority vote. The ROI is heuristically defined as the extent of all atlas labels after linear registration to the template, dilated by three voxels (?). The number of top ranked template library image labels is a configurable parameter.

The `xcorr_vol` utility from the ANIMAL toolkit is used to calculate the cross-correlation similarity measure.

2.4.3 Normalised Mutual Information Weighted Majority Vote

This method is similar to cross-correlation weighted voting except that image similarity is calculated by the normalised mutual information score over the region of interest(Studholme et al., 2001). The `itk_similarity` utility from the EZMinc toolkit[3] is used to calculate the normalised mutual information measure between to images.

2.5 Assessing Segmentation Agreement

The Dice similarity coefficient (DSC) assesses the agreement between two segmentations. It is one of the most widely used measures of segmentation performance, and we use it as the basis of comparison throughout this paper. Additionally, we report the Jaccard index, another commonly used similarity measure:

$$\text{Dice's coefficient (DSC)} = \frac{2|A \cap B|}{|A| + |B|}$$

$$\text{Jaccard (J)} = \frac{|A \cap B|}{|A \cup B|} = \frac{DSC}{(2 - DSC)}$$

where A and B are the regions being compared, and the cardinality is the volume measured in voxels.

2.6 Experiments

The following experiments were performed to assess the performance of MAGeT brain with various parameter settings as well as on diverse datasets. In each experiment we contrast the performance of MAGeT brain with that standard single- and multi-atlas segmentations derived from the same atlas library.

2.6.1 ADNI1 cross-validation

To test the effect of parameter settings on the MAGeT brain algorithm, Monte Carlo Cross-Validation (MCCV) (?) was performed using a subset of the ADNI1 subjects for validation. This form of cross-validation (described in detail below) allows us to validate MAGeT with various atlas and template library sizes, registration and label fusion methods.

Dataset evaluated. 69 1.5T images were arbitrarily selected from the *ADNI1:Screening 1.5T* standardized dataset. 23 subjects were chosen from each disease category (cognitively normal (CN), MCI and AD). Demographics for this subset are shown in Table 4.

Atlas and template libary. Atlases consist of images taken from the dataset, with corresponding manual labels provided by SNT. Atlas library size varied from 3 to 9 images. The remaining 60-66 target

---

[3] https://github.com/vfonov/EZminc

Table 4: ADNI-1 cross-validation subset demographics

	CN	LMCI	AD	Combined
	$N = 23$	$N = 23$	$N = 23$	$N = 69$
Age at baseline Years	72.2 75.5 78.5	71.0 77.1 81.4	71.7 77.8 81.8	71.5 76.6 81.3
Sex : Female	43% (10)	43% (10)	43% (10)	43% (30)
Education	16.0 16.0 18.0	15.0 16.0 18.0	12.0 16.0 16.5	14.0 16.0 18.0
Ethnicity : Unknown	0% (0)	0% (0)	0% (0)	0% (0)
Not Hisp/Latino	100% (23)	100% (23)	100% (23)	100% (69)
Hisp/Latino	0% (0)	0% (0)	0% (0)	0% (0)
CDR-SB	0.00 0.00 0.00	0.75 1.50 1.50	4.00 4.50 5.00	0.00 1.50 4.00
ADAS 13	4.67 5.67 12.34	14.34 16.00 20.50	23.83 29.00 31.66	10.00 16.00 25.33
MMSE	28.5 29.0 30.0	25.0 27.0 28.0	21.0 23.0 24.0	24.0 27.0 29.0

a b c represent the lower quartile a, the median b, and the upper quartile c for continuous variables.
Numbers after percents are frequencies.

images were segmented with the template library size varying from 3 to 20 images for each setting of atlas library size. Template library images were selected at random from the targets.

Registration method. Both the ANTS and ANIMAL registration methods were used.

Label fusion. Majority vote, cross-correlation weighted majority vote, and Normalized Mutual Information weighted majority vote were used. With the weighted majority vote fusion methods, the number of top labels used in the fusion was varied from 3 to 20 images.

Evaluation. Monte Carlo Cross-Validation (MCCV), also known as repeated random sub-sampling cross-validation, consists of repeated trials in which items from the dataset are randomly sampled (without replacement) and assigned to a training set or validation set **?**.

In each trial, the training set consists of images and SNT labels used as atlases, and the validation set consists of images to be segmented along with the corresponding SNT labels used as gold-standard segmentations. Both MAGeT brain and basic multi-atlas segmentation were performed in each trial, and the accuracy of the resulting segmentations were measured against the SNT labels.

We performed 10 trials on each combination of parameters listed above: atlas library size (1-9), template library size (1-20), registration method (ANTS vs. ANIMAL), and label fusion method (MV, XC-WV, NMI-WV). A total of 1080 parameter settings were evaluated over a total of trials.

2.6.2 ADNI-1 Screening Validation

To test the accuracy of MAGeT brain on a real-world task we segment the entire ADNI-1 dataset using an atlas set that is not representative of the target set.

Dataset evaluated. All images from the *ADNI1:Screening 1.5T* standardized dataset.

Atlas and template libary. The Winterburn atlases were used as the atlas library. The template library consisted of 21 randomly selected images from the ADNI1 data dataset (7 healthy, MCI and AD subjects).

Registration method. The ANTS non-linear registration algorithm was used, as it performed best in the ADNI1 cross-validation experiment (see Results).

Label fusion. Majority vote was used performed equally well in the ADNI1 cross-validation experiment and is the easiest label fusion method to operate.

Evaluation. Since the hippocampal segmentation protocols differ between the ADNI labels and Winterburn atlases, this poses a problem for direct similarity comparisons between labels produced by MAGeT brain and the ADNI labels. To evaluate the performance of MAGeT brain, we compare the correlation of MAGeT segmentation volumes with manual segmentation (SNT) volumes. Additionally, we correlate the hippocampal volumes of established automated segmentation methods to MAGeT segmentations.

Additionally, we compared classification accuracy of subjects by diagnosis based on hippocampal volume using both the SNT labels and our produced labels.

Table 5: Multi-atlas means

merge	Atlases	ANTS	ANIMAL
1	3.00	0.81	0.76
2	4.00	0.79	0.75
3	5.00	0.82	0.79
4	6.00	0.82	0.78
5	7.00	0.83	0.80
6	8.00	0.83	0.79
7	9.00	0.84	0.80

2.6.3 SZ First Episode Patient Validation

Dataset evaluated. To validate that MAGeT performance generalises to across disease categories, we measure the performance of MAGeT on the Schizophrenic First Episode Patient (SFEP) dataset.

Atlas and template libary. - two different atlas sets: a manual hippocampal segmentation of patients, and Winterburn atlas set.

Registration method. ANTS.

Label fusion. Majority vote.

Evaluation. We validate the FEP-atlas segmentations using Dice's Kappa, and the Winterburn-atlas segmentations by correlating volumes.

complete

complete

complete

complete

2.6.4 Winterburn Atlases Validation

Dataset evaluated. - T1 BRAVO scans of the same subjects included in the Winterburn atlas set. These scans are taken within .... weeks of the scans for the Winterburn atlases.

Atlas and template libary. - Atlas library is Winterburn T1 atlases. Template library consists of all five T1 BRAVOs, plus 15 T1 healthy control images.

Registration method. ANTS

Label fusion. Majority vote.

Evaluation. - Leave one out cross-validation (LOOCV) in which all five subjects are segmented in separate runs of MAGeT brain. In each run, the subject to be segmented is excluded from the Atlas library (so only four atlases are used).

Segmentation accuracy is judged by difference in hippocampal volume.

complete

complete

complete

complete

complete

3 Results

3.1 ADNI-1 Cross-Validation

- find significant improvement over multi-atlas performed with the same parameters. Also, find smoothed performance is monotonically increasing but asymptotic in size of both template and atlas library, with peak performance reached after 15 templates.

- True for all parameter settings! (so works generally..)

Ideas:

- more atlases -¿ better performance

- larger template library -¿ better performance, but tails off around 10-15 templates

- no significant difference between majority or weighted vote methods (haven???t tested this statistically though).

- consistently performs better than average naive performance by XXX

Can we statis capture what performance thing like, th at which gain statistically i cant?
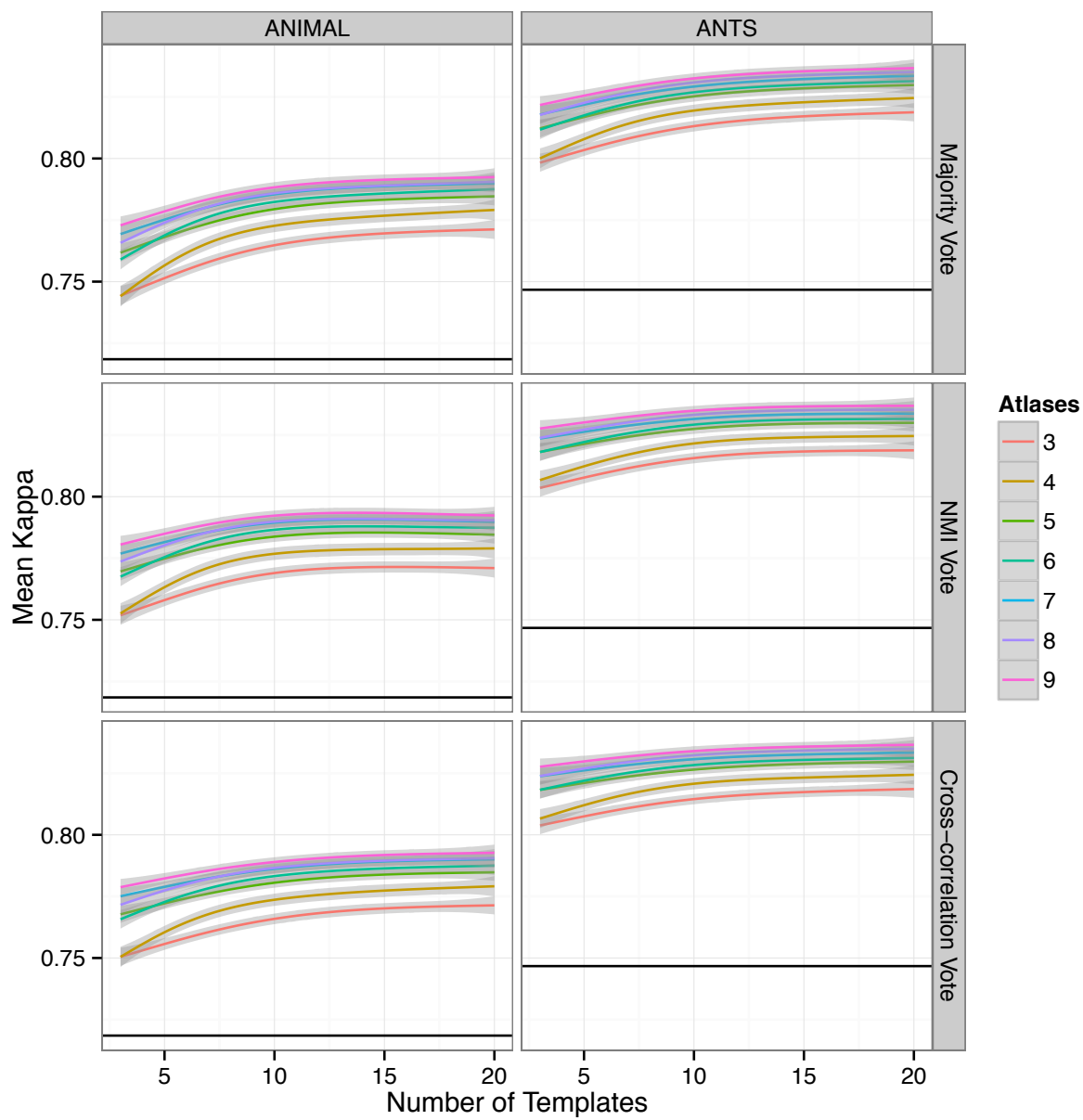
9

Figure 1: Comparison of MAGeT performance on ADNI-1 subset. Smoothing line fitted using GAM (generalised additive model) from R with defaults from ggplot2 (formula: y   s(x, bs = "cs"))
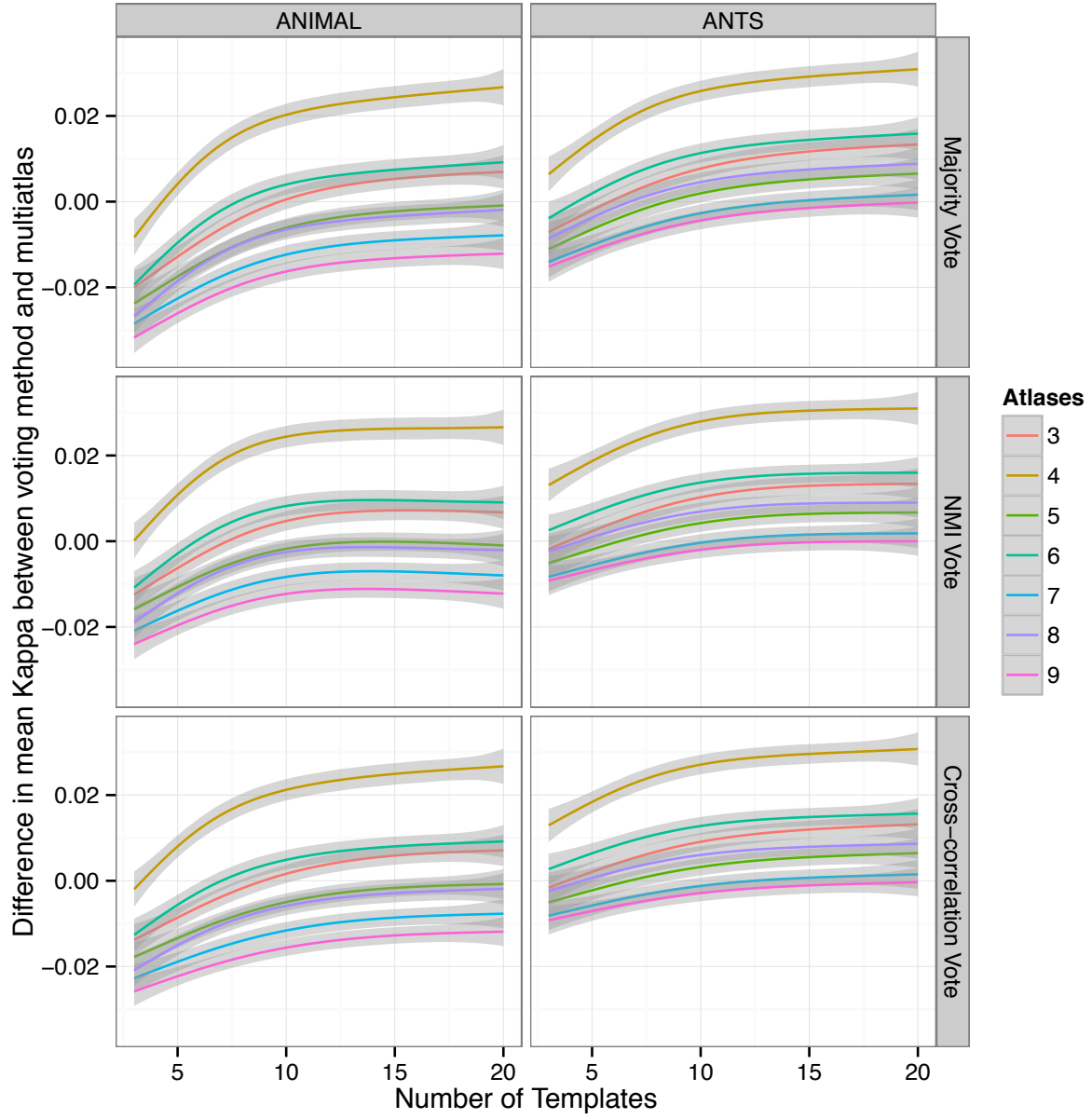
Figure 2: Difference in mean Kappa between MAGeT brain and multi-atlas

- using ANTS, with a large enough template library (¿12) MAGeT brain performs better than the average multi-atlas approach with the same number of atlases. using ANIMAL, 5 or more atlases needed before boost seen.

- more atlases -¿ smaller template library required to improve on average multi-atlas performance

- discuss variance? best/worst case? –how often do we expect random template library selection to work decently

3.2 ADNI-1 Screen Validation

Ideas:

- A2A shows that if atlas population strongly(?) represents subject set variability, then free choice from atlas population will produce improvements (we know this b/c of extensive validation trials).

- what about in the case where atlas population doesn???t strongly represent subject set variability (e.g. a priori atlas set)? then, we can use atlas selection to refine atlas set?

3.3 First Episode Schizophrenic Patients

High volume correlation between Winterburn segmentation volumes and ground truth. (High-ish?) Kappa when using manual segmentations as Atlases.

3.4 Winterburn Atlases Validation

4 Discussion

5 Conclusion

References

P Aljabar, R a Heckemann, a Hammers, J V Hajnal, and D Rueckert. Multi-atlas based segmentation of brain images: atlas selection and its effect on accuracy. *NeuroImage*, 46(3):726–38, July 2009. ISSN 1095-9572. doi: 10.1016/j.neuroimage.2009.02.018. URL http://www.ncbi.nlm.nih.gov/pubmed/19245840.

Owen T Carmichael, Howard A Aizenstein, Simon W Davis, James T Becker, Paul M Thompson, Carolyn Cidis Meltzer, and Yanxi Liu. Atlas-based hippocampus segmentation in Alzheimer's disease and mild cognitive impairment. *NeuroImage*, 27(4):979–90, October 2005. ISSN 1053-8119. doi: 10.1016/j.neuroimage.2005.05.005. URL http://www.pubmedcentral.nih.gov/articlerender.fcgi?artid=2862692&tool=pmcentrez&rendertype=abstract.

G E Christensen, S C Joshi, and M I Miller. Volumetric transformation of brain anatomy. *IEEE transactions on medical imaging*, 16(6):864–77, December 1997. ISSN 0278-0062. doi: 10.1109/42.650882. URL http://ieeexplore.ieee.org/xpl/articleDetails.jsp?arnumber=650882.

D L Collins, P Neelin, T M Peters, and A C Evans. Automatic 3D intersubject registration of MR volumetric data in standardized Talairach space. *Journal of computer assisted tomography*, 18(2):192–205. ISSN 0363-8715. URL http://www.ncbi.nlm.nih.gov/pubmed/8126267.

D Louis Collins and Jens C Pruessner. Towards accurate, automatic segmentation of the hippocampus and amygdala from MRI by augmenting ANIMAL with a template library and label fusion. *NeuroImage*, 52 (4):1355–66, October 2010. ISSN 1095-9572. doi: 10.1016/j.neuroimage.2010.04.193. URL http://www.ncbi.nlm.nih.gov/pubmed/20441794.

D. Louis Collins, C. J. Holmes, T. M. Peters, and A. C. Evans. Automatic 3-D model-based neuroanatomical segmentation. *Human Brain Mapping*, 3(3):190–208, October 1995. ISSN 10659471. doi: 10.1002/hbm. 460030304. URL http://doi.wiley.com/10.1002/hbm.460030304.

T den Heijer, F Van der Lijn, M W Vernooij, M de Groot, P J Koudstaal, a Van der Lugt, G P Krestin, a Hofman, W J Niessen, and M M B Breteler. Structural and diffusion MRI measures of the hippocampus and memory performance. *NeuroImage*, 63(4):1782–9, December 2012. ISSN 1095-9572. doi: 10.1016/j. neuroimage.2012.08.067. URL http://www.ncbi.nlm.nih.gov/pubmed/22960084.

Bruce Fischl, David H Salat, Evelina Busa, Marilyn Albert, Megan Dieterich, Christian Haselgrove, Andre van der Kouwe, Ron Killiany, David Kennedy, Shuna Klaveness, Albert Montillo, Nikos Makris, Bruce Rosen, and Anders M Dale. Whole brain segmentation: automated labeling of neuroanatomical structures in the human brain. *Neuron*, 33(3):341–55, January 2002. ISSN 0896-6273. URL http://www.ncbi.nlm. nih.gov/pubmed/11832223.

E. Geuze, E. Vermetten, and J D Bremner. MR-based in vivo hippocampal volumetrics: 2. Findings in neuropsychiatric disorders. *Molecular Psychiatry*, 10(2):160, September 2004. doi: 10.1038/sj.mp.4001579. URL http://www.nature.com.myaccess.library.utoronto.ca/mp/journal/v10/n2/full/4001579a. htmlhttp://www.nature.com.myaccess.library.utoronto.ca/mp/journal/v10/n2/pdf/4001579a. pdf.

Nitin Gogtay, Tom F Nugent, David H Herman, Anna Ordonez, Deanna Greenstein, Kiralee M Hayashi, Liv Clasen, Arthur W Toga, Jay N Giedd, Judith L Rapoport, and Paul M Thompson. Dynamic mapping of normal human hippocampal development. *Hippocampus*, 16(8):664–72, January 2006. ISSN 1050-9631. doi: 10.1002/hipo.20193. URL http://www.ncbi.nlm.nih.gov/pubmed/16826559.

Alexander Hammers, Richard Allom, Matthias J Koepp, Samantha L Free, Ralph Myers, Louis Lemieux, Tejal N Mitchell, David J Brooks, and John S Duncan. Three-dimensional maximum probability atlas of the human brain, with particular reference to the temporal lobe. *Human brain mapping*, 19(4):224–47, August 2003. ISSN 1065-9471. doi: 10.1002/hbm.10123. URL http://www.ncbi.nlm.nih.gov/pubmed/12874777.

Rolf A. Heckemann, Joseph V. Hajnal, Paul Aljabar, Daniel Rueckert, and Alexander Hammers. Automatic anatomical brain MRI segmentation combining label propagation and decision fusion. *NeuroImage*, 46 (3):726–38, July 2006. ISSN 1095-9572. doi: 10.1016/j.neuroimage.2009.02.018. URL http://www.ncbi. nlm.nih.gov/pubmed/19245840.

Rolf A Heckemann, Shiva Keihaninejad, Paul Aljabar, Katherine R Gray, Casper Nielsen, Daniel Rueckert, Joseph V Hajnal, and Alexander Hammers. Automatic morphometry in Alzheimer's disease and mild cognitive impairment. *NeuroImage*, 56(4):2024–37, July 2011. ISSN 1095-9572. doi: 10.1016/j.neuroimage. 2011.03.014. URL http://www.pubmedcentral.nih.gov/articlerender.fcgi?artid=3153069&tool= pmcentrez&rendertype=abstract.

Yuan-Yu Hsu, Norbert Schuff, An-Tao Du, Kevin Mark, Xiaoping Zhu, Dawn Hardin, and Michael W Weiner. Comparison of automated and manual MRI volumetry of hippocampus in normal aging and dementia. *Journal of magnetic resonance imaging : JMRI*, 16(3):305–10, September 2002. ISSN 1053-1807. doi: 10.1002/jmri.10163. URL http://www.pubmedcentral.nih.gov/articlerender.fcgi? artid=1851676&tool=pmcentrez&rendertype=abstract.

Clifford R Jack, Frederik Barkhof, Matt A Bernstein, Marc Cantillon, Patricia E Cole, Charles Decarli, Bruno Dubois, Simon Duchesne, Nick C Fox, Giovanni B Frisoni, Harald Hampel, Derek L G Hill, Keith Johnson, Jean-François Mangin, Philip Scheltens, Adam J Schwarz, Reisa Sperling, Joyce Suhy, Paul M Thompson, Michael Weiner, and Norman L Foster. Steps to standardization and validation of hippocampal volumetry as a biomarker in clinical trials and diagnostic criterion for Alzheimer's disease. *Alzheimer's & dementia : the journal of the Alzheimer's Association*, 7(4):474–485.e4, July 2011. ISSN 1552-5279. doi: 10.1016/j.jalz.2011.04.007. URL http://www.ncbi.nlm.nih.gov/pubmed/21784356.

Meghana S Karnik-Henry, Lei Wang, Deanna M Barch, Michael P Harms, Carolina Campanella, and John G Csernansky. Medial temporal lobe structure and cognition in individuals with schizophrenia and in their non-psychotic siblings. *Schizophrenia research*, 138(2-3):128–35, July 2012. ISSN 1573-2509. doi: 10.1016/ j.schres.2012.03.015. URL http://www.ncbi.nlm.nih.gov/pubmed/22542243.

Kelvin K Leung, Josephine Barnes, Gerard R Ridgway, Jonathan W Bartlett, Matthew J Clarkson, Kate Macdonald, Norbert Schuff, Nick C Fox, and Sebastien Ourselin. Automated cross-sectional and longitudinal hippocampal volume measurement in mild cognitive impairment and Alzheimer's disease. *NeuroImage*, 51(4):1345–59, July 2010. ISSN 1095-9572. doi: 10.1016/j.neuroimage. 2010.03.018. URL http://www.pubmedcentral.nih.gov/articlerender.fcgi?artid=2873209&tool= pmcentrez&rendertype=abstract.

Katherine L. Narr, Theo G.M. van Erp, Tyrone D. Cannon, Roger P. Woods, Paul M. Thompson, Seonah Jang, Rebecca Blanton, Veli-Pekka Poutanen, Matti Huttunen, Jouko Lönnqvist, Carl-Gustav Standerksjöld-Nordenstam, Jaakko Kaprio, John C. Mazziotta, and Arthur W. Toga. A Twin Study of Genetic Contributions to Hippocampal Morphology in Schizophrenia. *Neurobiology of Disease*, 11(1):83– 95, October 2002. ISSN 09699961. doi: 10.1006/nbdi.2002.0548. URL http://dx.doi.org/10.1006/ nbdi.2002.0548.

Katherine L Narr, Paul M Thompson, Philip Szeszko, Delbert Robinson, Seonah Jang, Roger P Woods, Sharon Kim, Kiralee M Hayashi, Dina Asunction, Arthur W Toga, and Robert M Bilder. Regional specificity of hippocampal volume reductions in first-episode schizophrenia. *NeuroImage*, 21(4):1563–75, April 2004. ISSN 1053-8119. doi: 10.1016/j.neuroimage.2003.11.011. URL http://www.ncbi.nlm.nih. gov/pubmed/15050580.

Sean M Nestor, Erin Gibson, Fu-Qiang Gao, Alex Kiss, and Sandra E Black. A Direct Morphometric Comparison of Five Labeling Protocols for Multi-Atlas Driven Automatic Segmentation of the Hippocampus in Alzheimer's Disease. *NeuroImage*, November 2012. ISSN 1095-9572. doi: 10.1016/j.neuroimage.2012. 10.081. URL http://www.ncbi.nlm.nih.gov/pubmed/23142652.

Jordan Poppenk and Morris Moscovitch. A Hippocampal Marker of Recollection Memory Ability among Healthy Young Adults: Contributions of Posterior and Anterior Segments. *Neuron*, 72(6): 931–937, December 2011. ISSN 0896-6273. doi: 10.1016/j.neuron.2011.10.014. URL http://www. sciencedirect.com/science/article/pii/S089662731100924Xhttp://pdn.sciencedirect.com. myaccess.library.utoronto.ca/science?_ob=MiamiImageURL&_cid=272195&_user=994540&_pii= S089662731100924X&_check=y&_origin=article&_zone=toolbar&_coverDate=22-Dec-2011&view= c&originContentFamily=serial&wchp=dGLbVlV-zSkzk&md5=e75d94a1de9d5c31e146f910b38468da/ 1-s2.0-S089662731100924X-main.pdfhttp://www.sciencedirect.com.myaccess.library. utoronto.ca/science/article/pii/S089662731100924X.

Steven Robbins, Alan C Evans, D Louis Collins, and Sue Whitesides. Tuning and comparing spatial normalization methods. *Medical image analysis*, 8(3):311–23, September 2004. ISSN 1361-8415. doi: 10.1016/j.media.2004.06.009. URL http://www.ncbi.nlm.nih.gov/pubmed/15450225.

Mert R Sabuncu, Rahul S Desikan, Jorge Sepulcre, Boon Thye T Yeo, Hesheng Liu, Nicholas J Schmansky, Martin Reuter, Michael W Weiner, Randy L Buckner, Reisa a Sperling, and Bruce Fischl. The dynamics of cortical and hippocampal atrophy in Alzheimer disease. *Archives of neurology*, 68(8):1040–8, August 2011. ISSN 1538-3687. doi: 10.1001/archneurol.2011.167. URL http://www.pubmedcentral.nih.gov/ articlerender.fcgi?artid=3248949&tool=pmcentrez&rendertype=abstract.

W B Scoville and B Milner. Loss of recent memory after bilateral hippocampal lesions. 1957. *The Journal of neuropsychiatry and clinical neurosciences*, 12(1):103–113, 2000. URL http://www.ncbi.nlm.nih.gov/ pubmed/10678523.

J G Sled, a P Zijdenbos, and a C Evans. A nonparametric method for automatic correction of intensity nonuniformity in MRI data. *IEEE transactions on medical imaging*, 17(1):87–97, February 1998. ISSN 0278-0062. doi: 10.1109/42.668698. URL http://www.ncbi.nlm.nih.gov/pubmed/9617910.

C Studholme, E Novotny, I G Zubal, and J S Duncan. Estimating tissue deformation between functional images induced by intracranial electrode implantation using anatomical MRI. *NeuroImage*, 13(4):561–76, April 2001. ISSN 1053-8119. doi: 10.1006/nimg.2000.0692. URL http://www.ncbi.nlm.nih.gov/pubmed/11305886.

Robin Wolz, Paul Aljabar, Joseph V Hajnal, Alexander Hammers, and Daniel Rueckert. LEAP: learning embeddings for atlas propagation. *NeuroImage*, 49(2):1316–25, January 2010. ISSN 1095-9572. doi: 10.1016/j.neuroimage.2009.09.069. URL http://www.pubmedcentral.nih.gov/articlerender.fcgi?artid=3068618&tool=pmcentrez&rendertype=abstract.

Bradley T Wyman, Danielle J Harvey, Karen Crawford, Matt A Bernstein, Owen Carmichael, Patricia E Cole, Paul K Crane, Charles Decarli, Nick C Fox, Jeffrey L Gunter, Derek Hill, Ronald J Killiany, Chahin Pachai, Adam J Schwarz, Norbert Schuff, Matthew L Senjem, Joyce Suhy, Paul M Thompson, Michael Weiner, and Clifford R Jack. Standardization of analysis sets for reporting results from ADNI MRI data. *Alzheimer's & dementia : the journal of the Alzheimer's Association*, October 2012. ISSN 1552-5279. doi: 10.1016/j.jalz.2012.06.004. URL http://www.ncbi.nlm.nih.gov/pubmed/23110865.
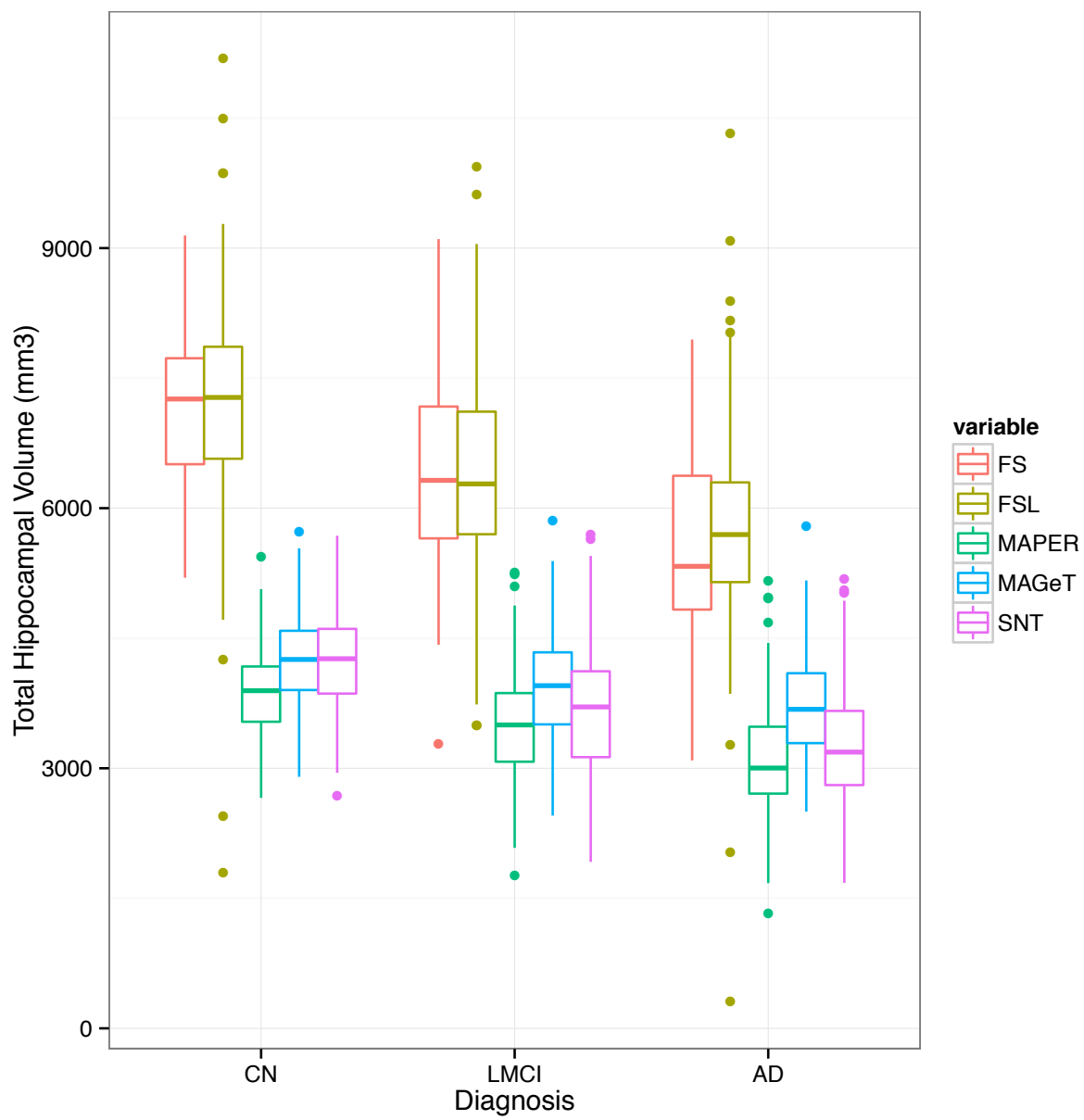
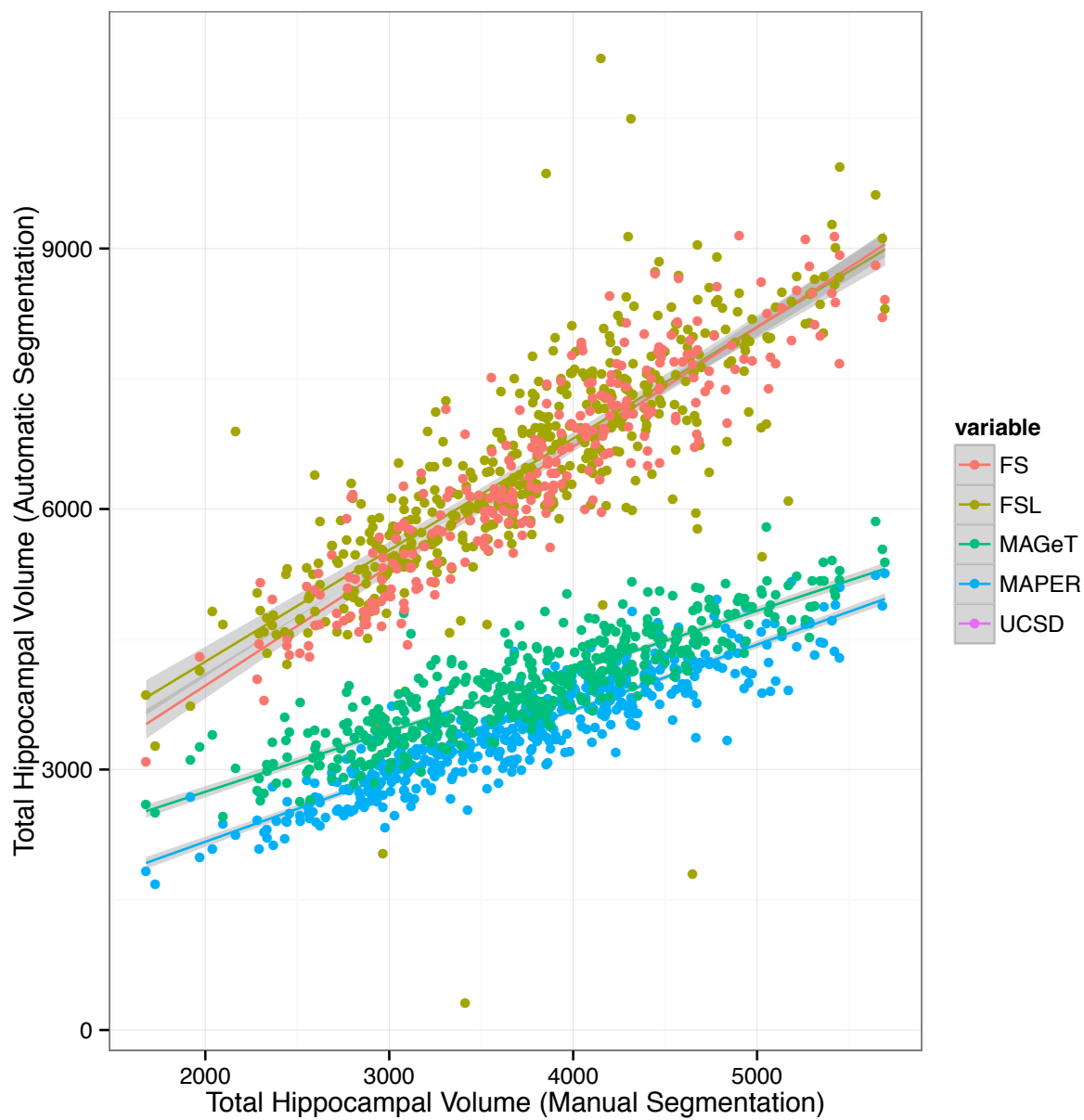Figure 3: Comparison of HC volumes by FreeSurfer (FSF), MAGeT brain (MAGeT), MAPER, and manual (SNT).

Figure 4: **ADNI Baseline cohort.** Comparison of HC volumes by FreeSurfer (FSF), MAGeT brain (MAGeT), MAPER, and manual (SNT).
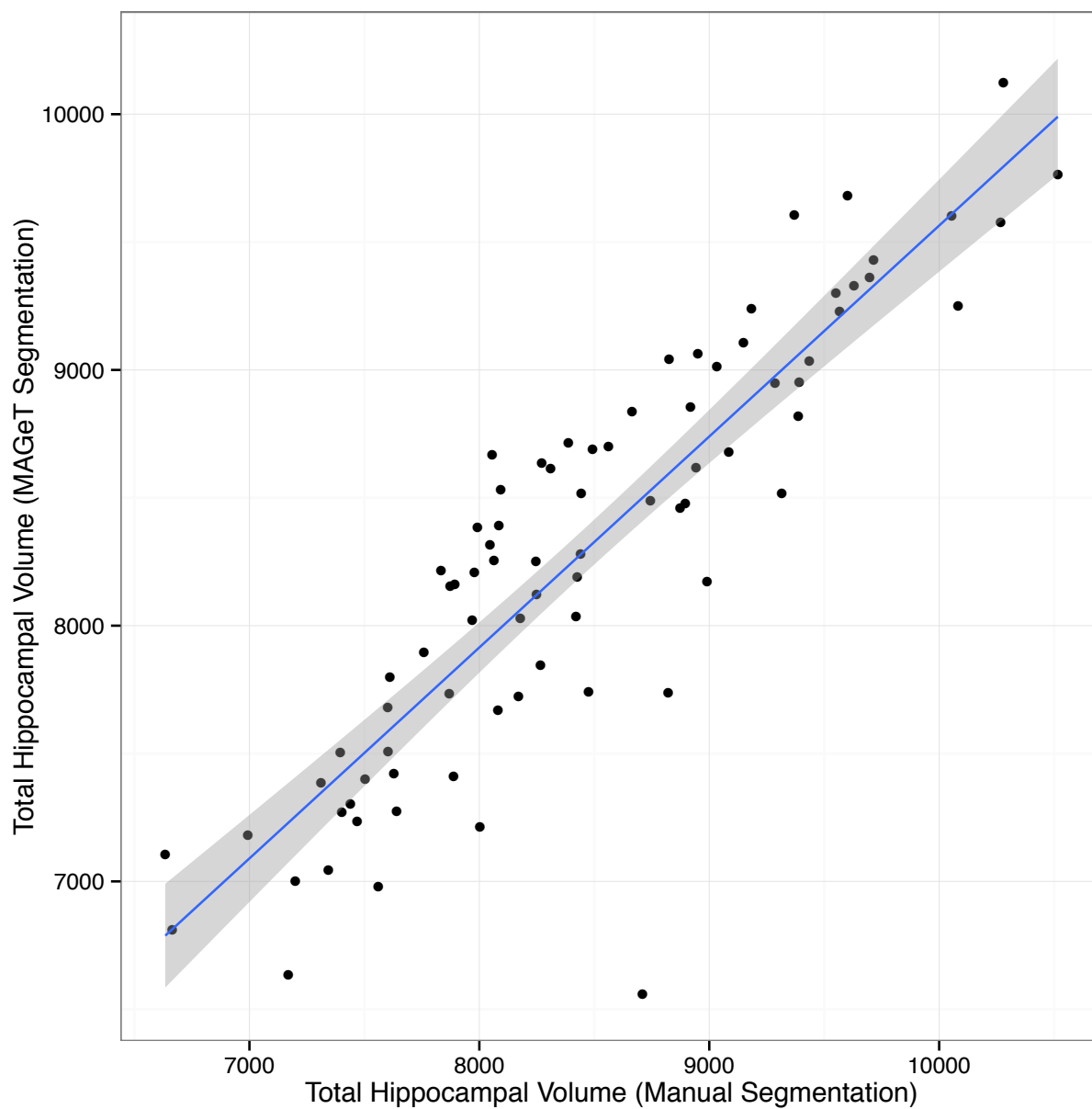
Figure 5: **First Episode Schizophrenic Patients.** Comparison of total HC volumes for MAGeT against manually rated Hippocampal volumes